Supporting Information

Direct epitaxial growth of polar $(1-x)HfO_2$-$(x)ZrO_2$ ultra-thin films on Silicon

Pavan Nukala[1,#,*], Jordi Antoja-Lleonart[1,#], Yingfen Wei[1], Lluis Yedra[2,3], Brahim Dkhil[2], Beatriz Noheda[1,*]

1. Zernike Institute of Advanced Materials, University of Groningen, 9747 AG, The Netherlands

2. Laboratoire Structures, Propriétés et Modélisation des Solides, CentraleSupélec, CNRS-UMR8580, Université Paris-Saclay, 91190 Gif-sur-Yvette, France
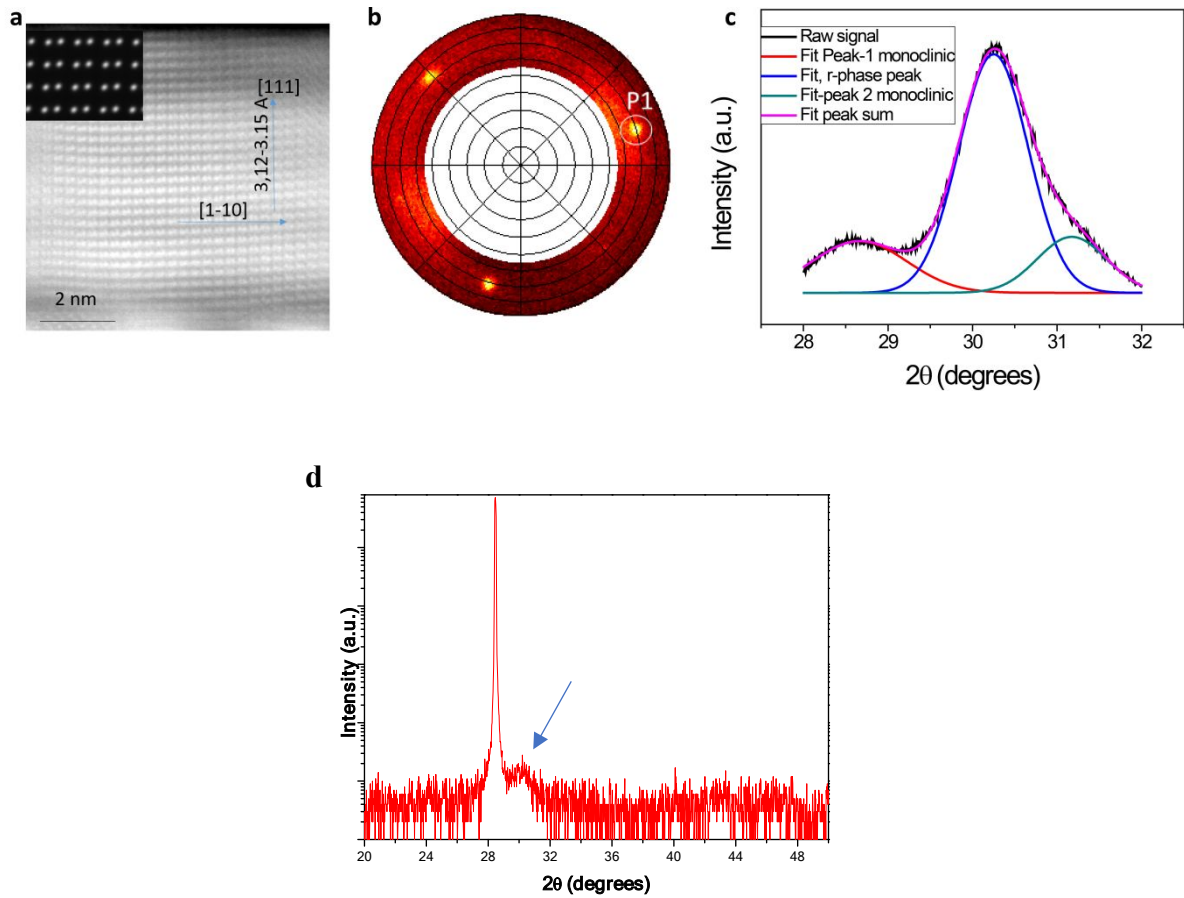
3. Laboratoire Mécanique des Sols, Structures et Matériaux, CentraleSupélec, CNRS UMR 8579, Université Paris-Saclay, 91190 Gif-sur-Yvette, France

* corresponding authors email: p.nukala@rug.nl, b.noheda@rug.nl

# equally contributing authors

Supplementary figures:

Figure S1: (a) HAADF image acquired along [-211] zone axis, $(1-x)HfO_2:(x)ZrO_2$ (HZO-x), x=0.5, clearly showing [111] texture. Inset shows the HAADF image simulation of the monoclinic phase (sample thickness=20 nm) in this zone , which matches with our experimental patterns very well. (b) Pole figure from HZO x=0.85, films grown on Si(111) around $2\theta\approx30^o$ corresponding to {111} planes of HZO. These figures look very similar to the ones obtained at x=0.5 and 0.7 compositions (Figure 1a in the main text), and are consistent with (111) oriented films. (c) Fitting procedure on the θ-2θ of P1 in (a) is shown here. The raw signal between $2\theta\approx28^o$ and 32° is fit to three Gaussians centered at 28.55^o (red, monoclinic {111}), 30.24^o (blue, low-volume phase {111}), and 31.20^o (green, monoclinic {11-1}). From these fits on all the three poles (P1-P3) and the out-of-plane peak (arrow in d), the ones corresponding to the low-volume phase are selectively shown in Figure 2a in the

main text. The 3:1 degeneracy in the {111} peaks of the low-volume phase clearly show that it is rhombohedral.
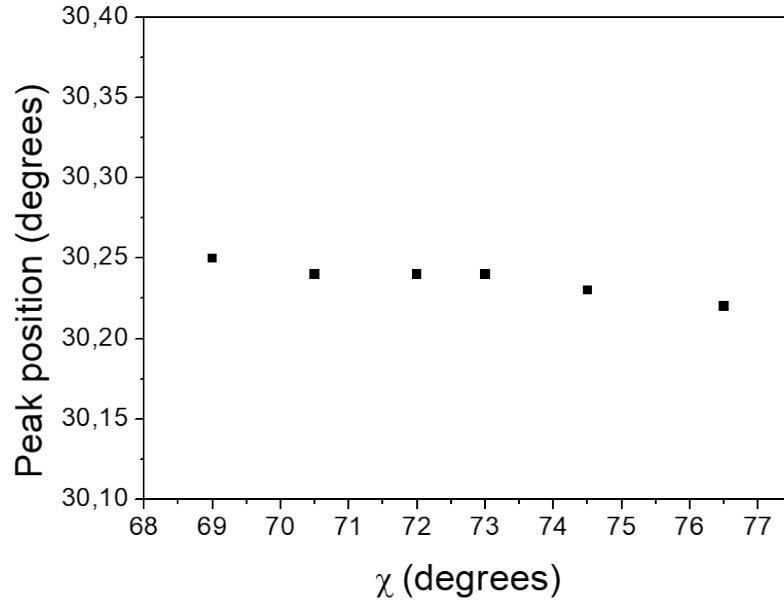
Figure S2. Error analysis in peak positions, as a function of misalignment and inhomogeneous strain.

Typically the alignment procedure for θ-2θ scans works on the basis of selecting the values of χ and φ (also θ-offset), at which the intensity of the Bragg spot is the maximum. However, changing from these conditions amounts to misalignment. Slight misalignments (i.e. in χ) can change the peak position of the low-volume peak owing to effects concerning inhomogeneous strains. This contributes to an error in the values of peak positions obtained from the Gaussian fittings. It is important to quantify this error, because our phase allocation depends completely on the degeneracy obtained from peak positions. In this figure, we quantify the changes in the peak positions of the low-volume phase that occur upon deliberate misalignment. θ-2θ scans were collected from P1 of Figure S1a in the HZO (x=0.85 sample) at various values of χ, and peak positions were obtained from a corresponding Gaussian fitting procedure of these scans (described in Figure S1). We do notice that the misalignment induces a spread in the values of peak positions by $\Delta(2\theta) = 0.06°$, which is the main source of error in

the determination of the peak position. In the manuscript, all the peak positions data are reported with such error analysis.
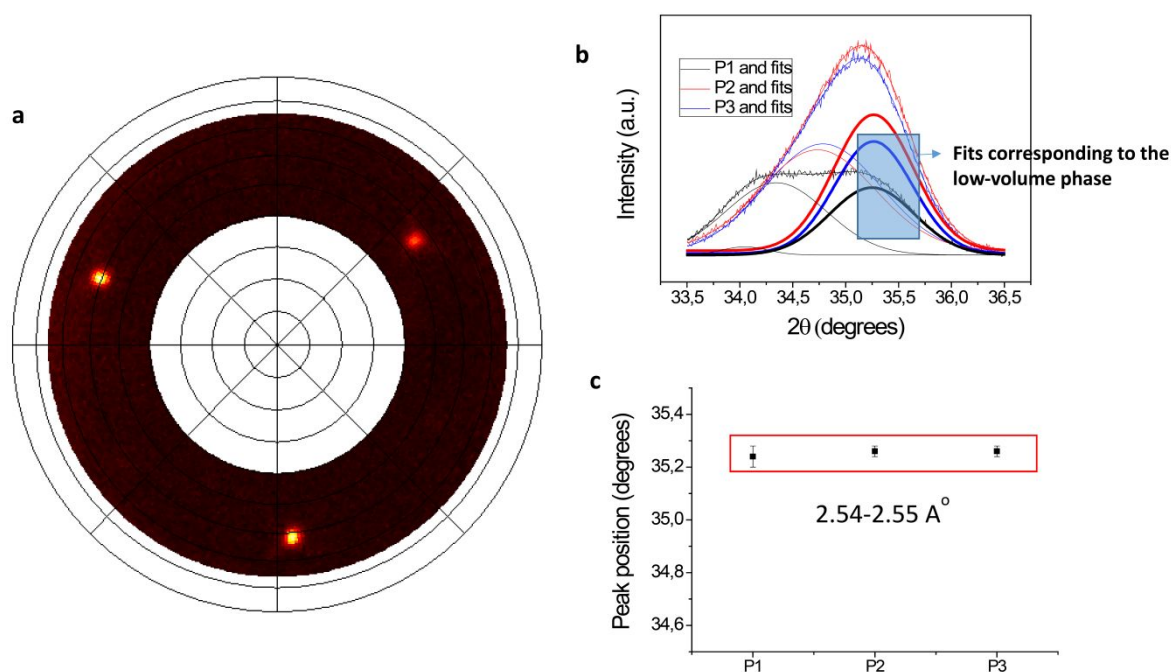
Figure S3. Pole figure and θ-2θ scans of the {001} poles on HZO (x=0.85) on Si (111)

(a)Pole figures collected about 2θ≈35º corresponding to the {001} peaks of HZO polymorphs. The three {001} poles are separated in φ by 120º and centered at χ≈56º. (b) θ-2θ scans show that every pole is a collection of a monoclinic phase peak(s) and a low-volume phase peak. Thus a two peak Gaussian fitting is done across all the scans. The full fit is shown together with the experimental data, to show the excellent quality of the fits. In addition the two separate peaks extracted from the fit are also plotted. Fits of the low-volume phase are highlighted by using thicker lines. (c) The peak positions obtained from the fits in the low-volume phase, reveal a unit cell with a=b=c of 5.08-5.10 Å . This, along with the {111} pole-figure analysis (Figure 2a, 2b in the manuscript) further confirms the r-phase symmetry (in r-

phase a=b=c). The commonly reported polar o-phase lattice parameters are 5.01, 5.24 and 5.11 Å, and are quite different from what we obtain here.
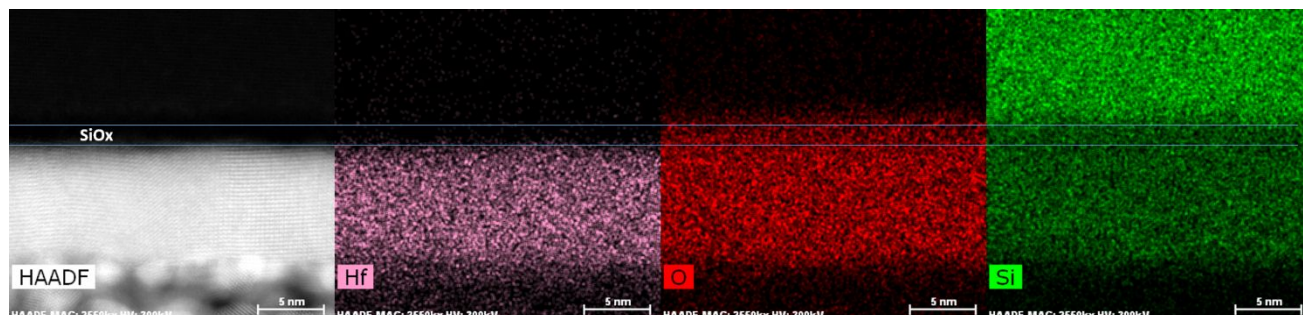
Figure S4. Representative EDS elemental maps of HZO (x=0.5) thin films

Hf, O, and Si elemental maps from obtained from a region shown in HAADF-STEM image on the left. These maps clearly show the existence of a contiguous a-SiO$_x$ (regrown) layer of < 1nm between the substrate and the film. The regrowth of a-SiO$_x$ in the later part of the growth process relaxes the strain on HZO stabilizing it in a bulk monoclinic phase. This is exactly what we see on these films with x=0.5. They completely stabilize in a monoclinic phase. On samples with x=0.7, we can clearly identify regions with and without regrown a-SiO$_x$. The film above the regions with a-SiO$_x$ is monoclinic, and without the regrown SiO$_x$ it is rhombohedral. Thus regrowth of a-SiO$_x$ seems to be predominant mode of strain relaxation in HZO systems.
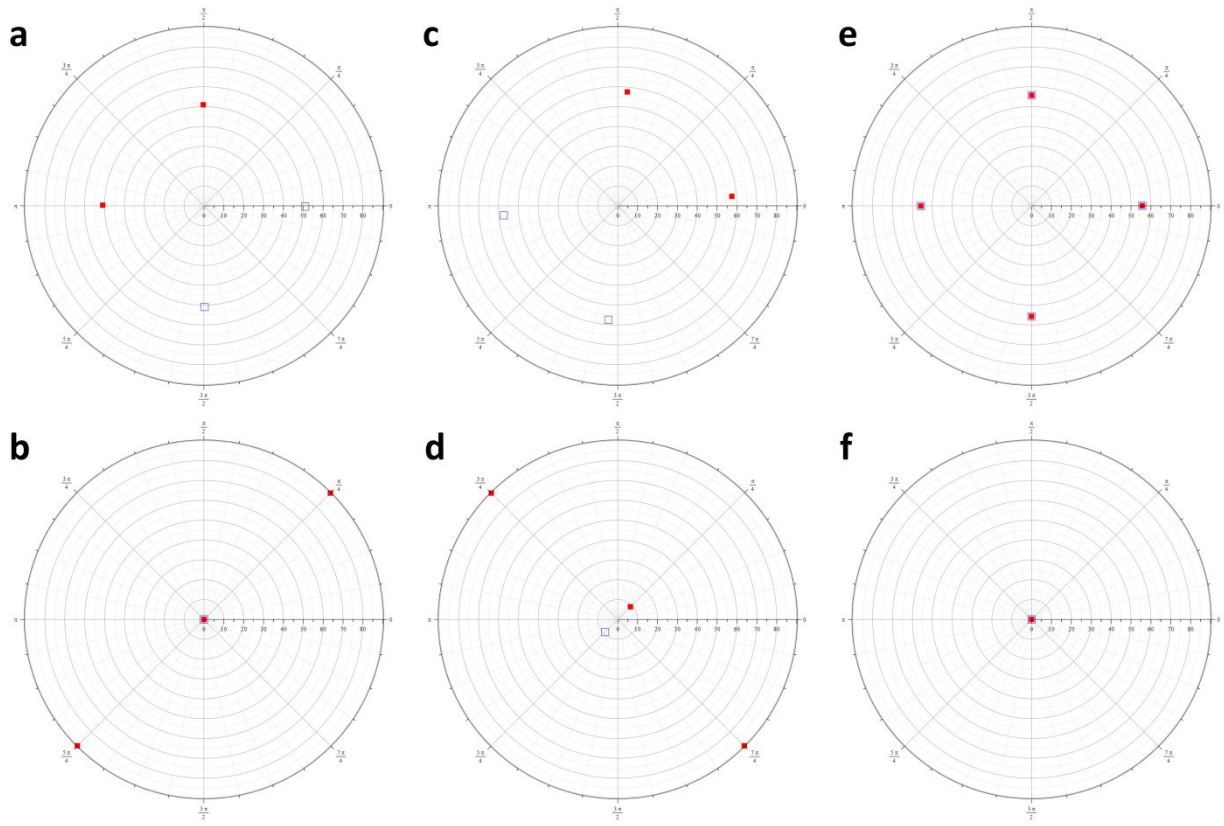
Figure S5. Predicted pole figures for the three proposed phases of HZO (x=0.7) on Si(100)

(a,b) Calculated pole figure for {111} family (a) obtained at $2\theta=31.71°$ and {100} family (b) obtained at 2θ between 34 and 35° for monoclinic domain of type 1, shown in Fig. 5c left panel. (c,d) Calculated pole figure for {111} family (c) and {100} family (d) for monoclinic domain of type 2, shown in Fig. 5c, center panel. (e,f) Calculated pole figure for {111} family (e) and {100} family (f) orthorhombic domains shown in Fig. 5c, right panel.

A simple mathematical model was used to generate the pole locations (in 2θ, χ, and φ) for the relevant Bragg peaks of m- and o-HZO, using the bulk lattice parameters of m-HfO$_2$ and o-ZrO$_2$ as a starting point (*Kisi, E.H., Howard, C.J., and Hill, R.J. Crystal structure of orthorhombic zirconia in partially stabilized zirconia. J. Am. Ceram. Soc. 72, 1757-1760 (1989).*). For each set of Miller indices, the d-spacing was calculated, as well as the reciprocal

space director vector for that plane family. Then, by keeping that vector's angles to a set of basis vectors constant, and rotating the basis by an arbitrary amount in χ and φ, the pole locations for any lattice plane of any m- and o-HZO domain could be calculated and plotted. Here a simple polar diagram is used; the experimental data in the manuscript uses equal area projections. Diffraction intensities were not included in the model.

Here we show the pole figures for one domain each of the types proposed in Figure 5c of the manuscript. The red squares indicate a pole on the northern hemisphere ($0 < \chi < 90$) and the blue boxes indicate one on the southern hemisphere ($90 < \chi < 180$) of the samples, thus not accessible in our measurements. Poles located in the equator are plotted in red for convenience, but in practice they are not visible in our experimental data. Only poles with 2θ values close to the ones for the measured pole figures are shown in the calculated ones.

The top row (a, c, e) displays the figures for the (111) plane family. In the monoclinic phase, this plane family shows four peaks near $2\theta=31.71^\circ$, shown here, and four more at $2\theta=28.49^\circ$. In the orthorhombic phase, all eight peaks are close to $2\theta=30.23^\circ$ (see Table 1). The bottom row (b, d, f) figures show the (002) plane family, in each case generating six peaks between 34° and 35°.

In all three proposed domain types, the b-axis is parallel to the a- or b-axis of the Si(100) substrate, For the first m-domain type (a, b), we additionally imposed that the ab plane be parallel to Si(001), i.e. we set the HZO(002) reflection to have $\chi=0$. For the second m-domain type (c, d) we set that same reflection to instead have $\chi=\beta-90^\circ$ while holding the HZO(200) at $\chi=90^\circ$, thus tilting the ab plane in such a way that the c-vector (in direct space) is pointing upward, exactly perpendicular to the Si(001) plane. For the o-domain (e, f), the a-axis is pointing upward perpendicular to the substrate surface.

The only remaining step is to rotate each of the calculated pole figures in φ by multiples of 90°, thus including the contributions for four (two in the orthorhombic case) in-plane domain orientations. This provides an excellent match with the measured pole locations, particularly

for the monoclinic cases, giving rise to our claim that in thin (5nm) samples the m-HZO phase has its ab plane parallel to the substrate. In thick (20nm) samples this is no longer the case, instead with its c-axis (in direct space)pointing perpendicular to the substrate. In intermediate (10nm) thickness a mix of all domain types is observed.
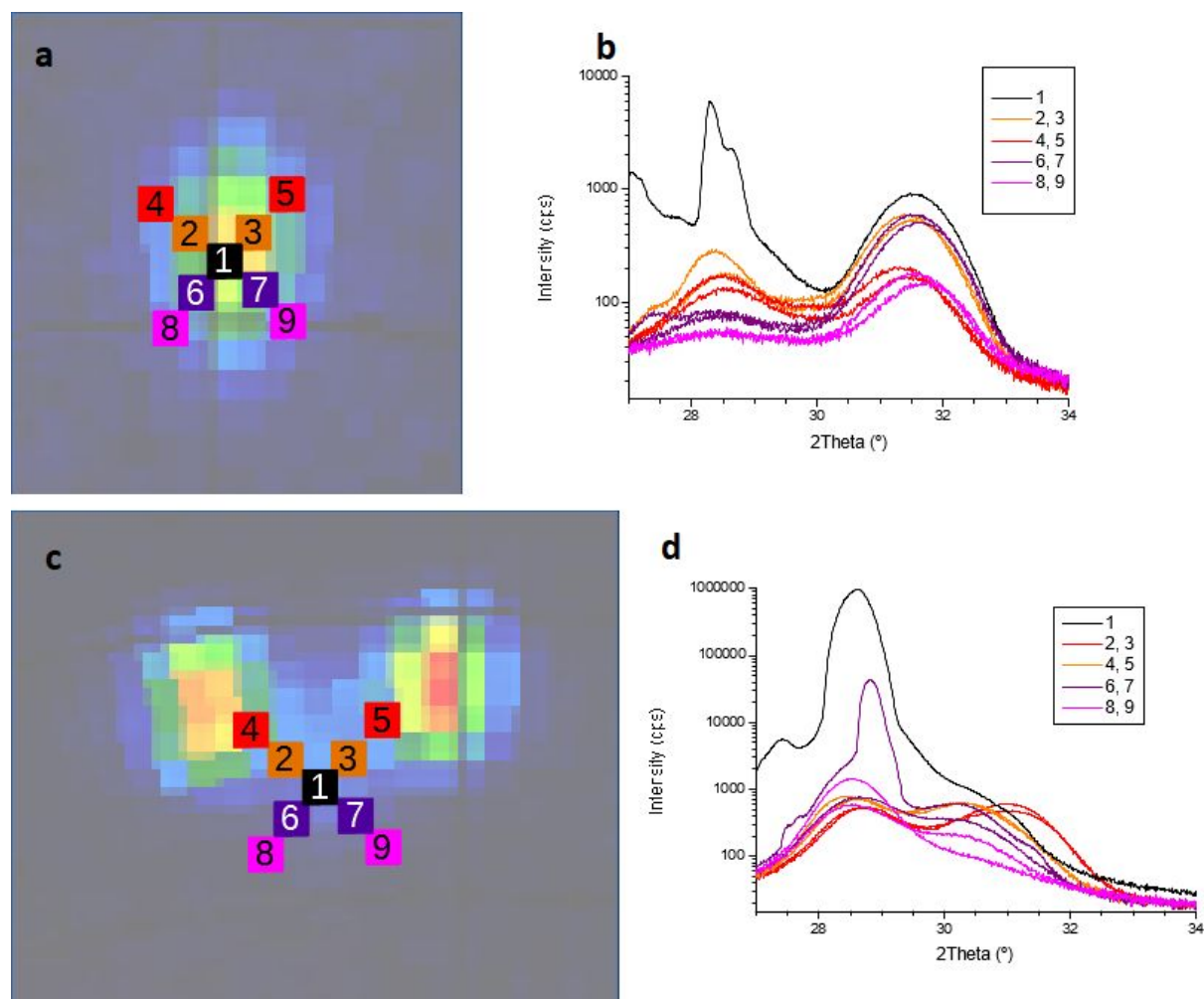
**Figure S6 : θ-2θ scans of 5nm- and 20nm-thick HZO (x=0.7) on Si(100).**

(a) A representative (111) pole of the 5 nm film of HZO (x=0.7) on Si(100). 1-9 indicate various pixels, each of them uniquely defined by (χ, φ). (b) θ-2θ scans at each of the 9 pixels for the pole shown in (a). (c) A representative (111) pole of the 20 nm film of HZO (x=0.7)

on Si(100). 1-9 indicate various pixels, each of them uniquely defined by (χ, φ). (d) θ-2θ scans at each of the 9 pixels for the pole shown in (d).

The (111) poles found in Figure 4 of the manuscript were analyzed by further θ-2θ scans. In particular, nine scans were performed near the (111) poles of the 5nm- and 20nm-thick films, in the positions indicated in a and c. The black pixel (no misalignment) was aligned using the Si(111) peak. The other pixels are misaligned by 1 or 2 degrees in χ and φ away from the black pixel. The results from scanning in all nine pixels are plotted in b and d, with the line colors matching those of the pixels for convenience.

For both cases. a similar behavior is observed to that of the 10nm-thick film. The signature of the low-volume phase is barely visible after scanning over the (111) pole of the 5nm film. However, in the 20nm film scanning results in a noticeable peak for the low-volume phase. It is possible that this low-volume phase somehow becomes more prevalent with increasing thickness. However, another convincing explanation is that, with increasing thickness, the fraction of the film that remains with its ab plane parallel to the Si(100) substrate decreases, thus weakening the peak at χ=54º enough that the low-volume peak becomes much more obvious.
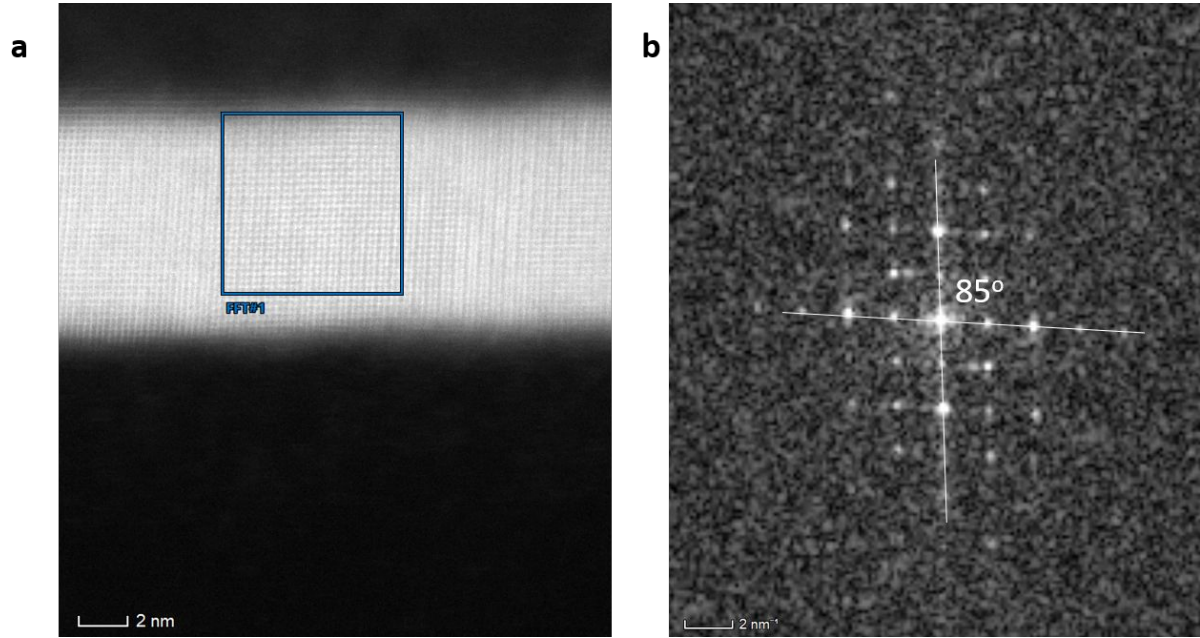
Figure S7: (a) HAADF-STEM image of HZO (x=0.7, t=10 nm) film on Si (100) (b) Fast Fourier Transform obtained from the blue boxed region in (a). The d-spacings correspond to a monoclinic phase. The monoclinic angle is β=95º. The spot corresponding to the ab plane is perfectly aligned with the substrate normal, or ab plane //Si (100). This kind of domain (Figure 5c in the manuscript) is predominant in the thinner sample (t=5 nm), and completely disappears in the thicker sample (t=20 nm). The most intense pixels from all the poles observed in the pole figures from HZO (x=0.7, t=5 nm, Figure 4 a,b) arise from these domains.
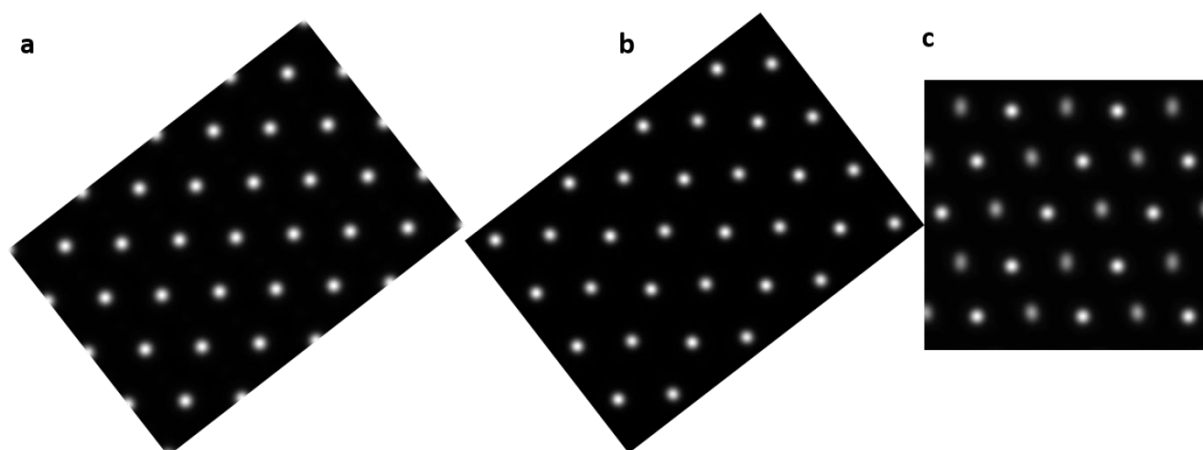
Figure S8: (a,b,c) HAADF multislice simulations (sample thickness=20 nm) of t-, o- and r3 phases. The horizontal direction is the <112> direction, and contrast changes in alternate cationic positions is only characteristic of an r-phase.